Sensors & Transducers Journal, Vol. 137, Issue 2, February 2012, pp. 176-188

www.sensorsportal.com

Sensors & Transducers

ISSN 1726-5479

http://www.sensorsportal.com

Nanostructured $MgFe_2O_4$ Thick Film Resistors as Ethanol Gas Sensors Operable at Room Temperature

*** S. V. BANGALE, S. R. BAMANE**

Metal Oxide Research, Laboratory, Department of Chemistry, Dr. Patangrao Kadam Mahavidyalaya, Sangli, 416416 (M.S.) India

Tel.: 0233-2535993, fax: 0233-2535993

E-mail: bangale_sv@rediffmail.com

Received: 3 December 2011 /Accepted: 14 February 2012 /Published: 28 February 2012

Abstract: Semiconductive nanoparticles of $MgFe_2O_4$ were synthesized by a solution combustion technique. This process is a convenient, environment friendly, inexpensive and efficient for the preparation of $MgFe_2O_4$ nanomaterial. The synthesized material is characterized by Thermo gravimetric Differential analysis (TG/DTA), X-ray Diffraction studied (XRD), Scanning Electron Microscopy (SEM) and Transmission Electron Microscopy (TEM) techniques. Conductance response of the nanocrystalline $MgFe_2O_4$ thick film is measured by exposing the film to reducing gases like ethanol, acetone, sulphur dioxide (H_2S), carbon dioxide (CO_2), and liquefied petroleum gas (LPG). The sensor exhibited a fast response and a good recovery. The results demonstrated that $MgFe_2O_4$ can be used as a gas-sensing material which has a high sensitivity and good selectivity to ethanol gas at 30 ppm. *Copyright © 2012 IFSA.*

Keyword: Nanostructured $MgFe_2O_4$, XRD, TEM, Ethanol gas sensors, Gas sensitivity.

1. Introduction

A spinel of the type M^{2+} $M_2^{3+}O_4$ attract the research interest because of their versatile practical application [1-2].Spinel ferrites with the general formula AFe_2O_4 (A = Mn,Co, Ni, Mg, or Zn) are very important magnetic materials because of their interesting magnetic and electrical properties with chemical and thermal stabilities [3]. Magnesium ferrite ($MgFe_2O_4$) is one of the most important ferrites. It has a cubic structure of normal spinel-type and is a soft magnetic n-type semiconducting material, which finds a number of applications in heterogeneous catalysis, adsorption, sensors, and in magnetic technologies [4-5]. Recently, nanostructures of magnetic materials have received more and

more attention due to their novel material properties that are significantly different from those of their bulk counterparts [6-9].Current years have been increased interests in study the gas sensing properties of ferrites [10-12]. Gopalreddy et al. reported the response of copper ferrite ($CuFe_2O_4$) and zinc ferrite ($ZnFe_2O_4$) for hydrogen sulfide (H_2S) and that of nickel ferrite ($NiFe_2O_4$) for chlorine gas (Cl_2). One of the present authors (Y-L.Liu) also confirmed that $ZnFe_2O_4$ possessed gas sensing properties for H_2S. magnesium ferrite ($MgFe_2O_4$) is one of the important ferrites with spinel structure [13]. It is used as a catalyst [14] and humidity sensor [15].It is also an n-type semiconductor with the band gap of 2.18V [16].

The need for a novel gas sensor capable of providing reliable operation in harsh environment is now greater than ever. Such sensors find a range of application, including the monitoring of traffic pollutants or food quality with specially designed electronic noses [17-18]. Gas sensors based on metal oxides are commonly used in the monitoring of toxic pollutants and can provide the necessary sensitivity, selectivity and stability required by such system [19]. Commonly used oxides include zinc oxide, titanium dioxide, iron oxide, tungsten oxide and tin oxide. These materials have successfully been employed to detect a range of gas vapours, particularly ethanol, methanol and propanol [20-21].

Ethanol is explosively utilized for beverages, industrial and scientific sectors. Ethanol is a hypnotic (sleep producer) [22] gas having toxic nature. Heavy exposure and/ or consumption of alcoholic beverage, particularly by smokers, increase the risk of cancer [23] of the upper respiratory and digestive tracks. Alcoholic cirrhosis leads to liver cancer. Amongst the women, the chances of breast cancer increase with alcoholic consumption or exposure. These working on ethanol synthesis have great chances of being victims of respiratory and digestive track cancer. So there is a great demand and emerging challenges for monitoring ethanol gas at trace level.

Among various materials used for sensing application, ferrite is used as a good class of sensing materials. But they suffer a drawback of being at higher temperature [24]. Consequently, it is interesting to investigate the gas-sensing properties of $MgFe_2O_4$. The gas sensing efficiency of the materials depends on its microstructural properties which are related to its method of preparation, the later plays a very important role with regard to the chemical, structural and properties of a spinel ferrite. $MgFe_2O_4$ is routinely synthesized by combustion method of precursors zinc nitrate, magnesium nitrate and glycine as fuel [25]. Alternatively, a number of wet method including coprecipitation [26], sol-gel [27], microemulsions [28], oxidation techniques [29] and hydrothermal synthesis [30]. An ideal process should be environmentally friendly and should be as simple as possible. A novel preparation technique of nanomaterial, combustion synthesis at ambient conditions, has been developed to prepared nanosized compounds. It was a high-yielding, low-cost and facile synthesis method. The mechanism of gas sensing involves surface reaction of the tin oxide surface with the test gas [31]. The ability to manipulate the surface of the nanocrystals by employing different synthetic routes has opened-up a new dimension to tailor material for specific properties application. Also, the sensitivity of the sensors depends on the method used to produce nanoparticles, with the efficiency of the chemical sensor increasing as particle size decreases [32-33].

The project describes a simple and cost-effective way of preparing of $MgFe_2O_4$ nanoparticles by auto combustion method using magnesium and ferric nitrates, glycine as fuel. Further it illustrates the structural, chemical composition, thermal morphology and gas sensing study of the samples using Thermo gravimetric Differential analysis (TG/DTA), X-ray diffraction (XRD), Fourier transform infrared spectroscopy (FT-IR),high-resolution scanning electron microscopy (HR-TEM), transmission electron microscopy (TEM), particle size analyzer and static gas sensing units to studied sensing properties.

2. Materials and Methods

2.1. Materials

All the reagents are of analytical grade and are used as received without further purification. Magnesium nitrate [$Mg(NO_3)_26H_2O$], ferric nitrate [$Fe(NO_3)_26H_2O$], glycine are purchased from Sigma-Aldrich chemical reagents Co. (USA).

2.2. Methods

In this study, $MgFe_2O_4$ powder was synthesized by solution combustion technique using the starting regents as $Mg(NO_3)_26H_2O$ (7.43 g), Fe $(NO_3)_26H_2O$ (7.27 g) and glycine (6.05 g) as a fuel. Glycine possesses a high heat of combustion. It is an organic fuel providing a platform for redox reactions during the course of combustion. Initially the magnesium nitrates, iron nitrates and glycine are taken in the 1:1:4 stoichiometric amount and homogenous paste was made. The paste formed was evaporated on hot plate in temperature range of 70 to 80 ^{0}C to result into a thick gel. The gel was kept on a hot plate for auto combustion and heated in the temperature range of 170 to 180 ^{0}C. The nanocrystalline$MgFe_2O_4$powder was formed within five minutes. The powder was sintered at 500, 600, 700, and 800 ^{0}C for 4 h, which resulted in to a brown color shining powder [34-35].

2.3. Thick Film Preparation

$MgFe_2O_4$powder was ground in an agate pastel-moter to ensure sufficiently fine particle size. The fine powder was calcined at 800 ^{0}C for 12 hr. in air and re-ground. The thixotropic paste was formulated by mixing the resulting $MgFe_2O_4$ fine powder with a solution of ethyl cellulose (a temporary binder) in a mixture of organic solvents turpineol. The ratio of inorganic ethyl cellulose and organic turpineol path was kept as 75:25 in formulating the paste. The paste was then used to prepare thick films. The thixotropic paste was screen printed on a glass substrate in desired patterns. The prepared films were fired at 550 ^{0}C for 24 h to the binder. The contacts were made by silver foil for electrical measurements.

2.4. Characterization

The as –prepared $MgFe_2O_4$ materials were characterized using TG/DTA thermal analyzer (SDT Q600 V 20.9 Build 20), X-ray diffract meter (PW-3710) using Cu-K_α radiation, Particle size analyzer, The TEM micrograph is obtained on a JEM 3010 (JEOL) transmission electron microscope with an accelerating voltage of 200 kV. Fourier transform infrared (FT-IR) spectrum is recorded on Perkin Elmer 2000 FT-IR spectrometer in KBr pellets. Microstructural characteristics such as morphology, particle size and crystal structure of the sample is analyzed by a high-resolution scanning electron microscope (JEOL JED 2300).

2.5. Fabrication and Analysis of Gas Sensors

The sensing performance of the sensors was examined using a “static gas-sensing system. There were electrical feeds through the base plate. The heating wire was fixed on the base plate to heat the sample under test up to the required operating temperatures. The current passing through the heating element was monitored using a relay with adjustable ON and OFF time intervals. Cr-Al thermocouple was used to sense the operating temperature of the sensors. The output of the thermocouple was connected to

digital temperature indicators. Gas inlet valve was fitted at one port of the base plate. The required gas concentration inside the static system was achieved by injecting a known volume of test gas using a gas-injecting syringe. Constant voltage was applied to the sensors, and current was measured by a digital Pico-ammeter. Air was allowed to pass into the glass dome after every gases exposure cycle as shown in Fig. 1 [36].

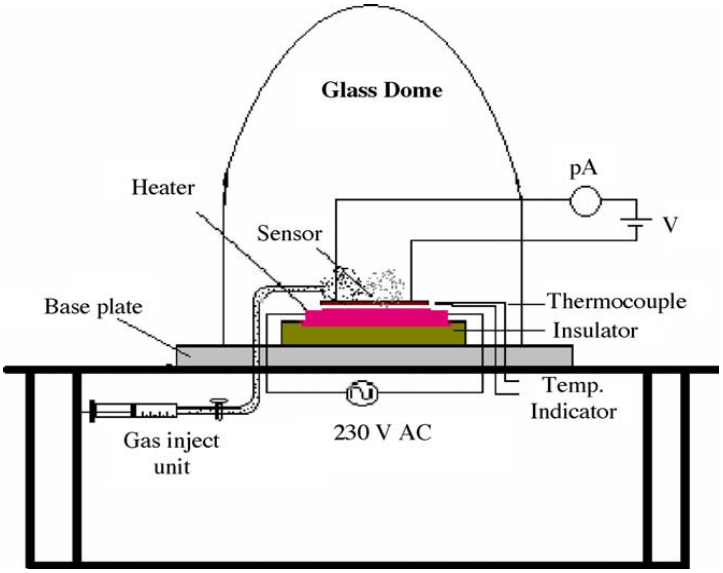

Fig. 1. Block diagram of static gas sensing system.

3. Result and Discussion

3.1. Spinel Structure and Formation Analysis

The TG curve in Fig. 2 shows a minor weight loss step (20 %) from 30 up to about 270 ^{0}C and two major weightloss steps from 270 to 455 ^{0}C (60 %) as shows in equation (1 and 2). No further weightloss was observed up to 1000 ^{0}C. The minor weight loss was related to the loss of moisture and trapped solvent (water and carbon dioxide) in the as-spun $MgFe_2O_4$ nanopowder, whereas the major weight loss was due to the combustion of organic matrix. On the DTA curve, main exothermic peaks were observed at ~290 and ~450 ^{0}C, suggesting the thermal events related to the decomposition of Mg and Fe nitratesalong with the degradation by dehydration on the nanopowder, which was confirmed by a dramatic weight loss in TG curve at the corresponding temperature range (270–455 ^{0}C). The plateau formed between 455 and 1000 ^{0}C on the TG curve indicated the formation of crystalline $MgFe_2O_4$ as the decomposition product as shown in Equation (1 and 2) [37-38]. As confirmed by XRD and FT-IR analyses as showed in Figures 3 and 6 respectively.

$$2C_2NH_3O_2 + (9/2)\ O_2 \rightarrow N_2\uparrow + 4CO_2\uparrow + 5H_2O\uparrow \quad (1)$$

$$Mg\ (NO_3)_3 + Fe\ (NO_3)_3 + 4C_2H5NO2 \rightarrow MgFe_2O_4 + 8CO_2\uparrow + 10H_2O\uparrow + 5N_2\uparrow \quad (2)$$

3.2. XRD Analysis

The XRD patterns of the calcined $MgFe_2O_4$ are shown in Fig. 3. All of the main peaks are indexed as the spinel $MgFe_2O_4$ in the standard data (JCPD No: 88-1935). The average crystallite sizes of $MgFe_2O_4$ samples were calculated from X-ray line broadening of the reflections of (220), (311), (400),

(511), and(440) using Scherrer's equation (i.e., D = 0.89 k/(βcosθ),where k is the wavelength of the X-ray radiation, K is a constant taken as 0.89, h the diffraction angle, and b is the full width at half-maximum [39-40] and were found to be16 ± 4, 18 ± 1, 25 ± 2, and 26 ± 3 nm for the samples of $MgFe_2O_4$calcined at 500, 600, 700, and 800 ^{0}C, respectively.

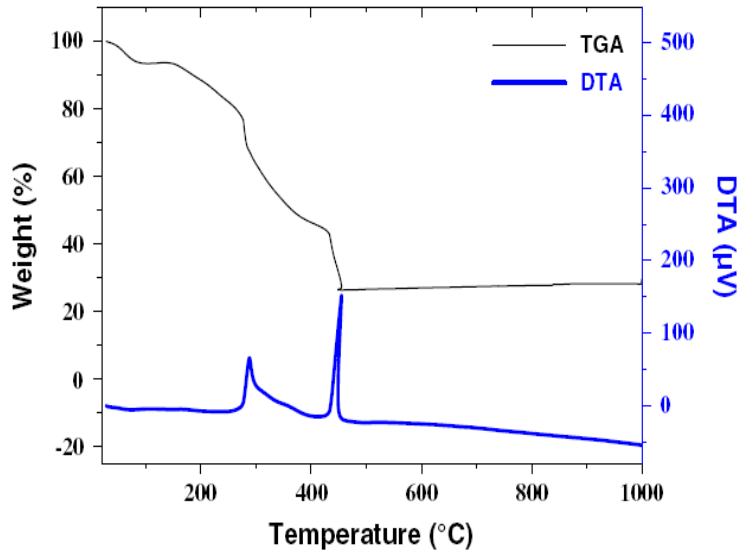

Fig. 2. Thermo gravimetric Differential analysis TG-DTA curve of mixed precursor$MgFe_2O_4$.

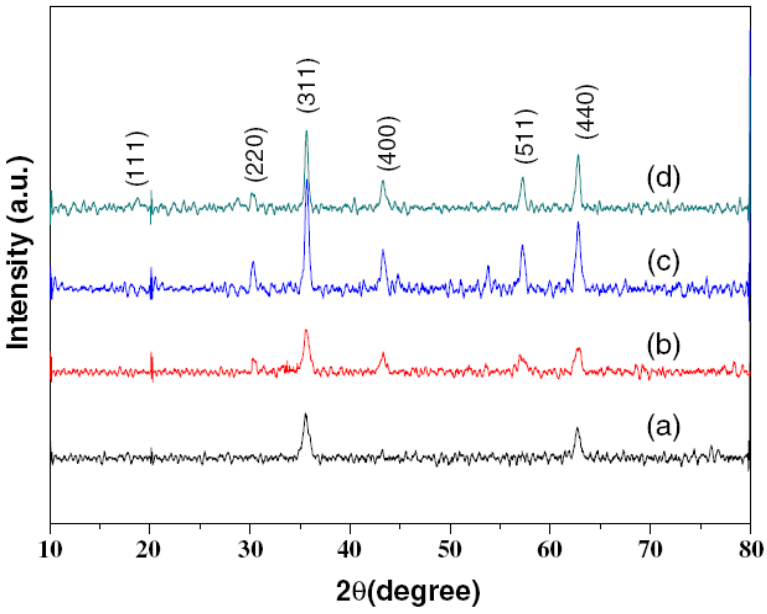

Fig. 3. XRD pattern of calcinied mixed precursor $MgFe_2O_4$at(a) 500 ^{0}C, (b) 600 ^{0}C, (c) 700 ^{0}C, and(d) 800 ^{0}C in air for 4 h.

3.3. Particle Size Distribution Analysis

Fig. 4 has been carried out by using dynamic light scattering techniques. (DLS *via* Laser input energy of 632 nm) It was observed that magnesium iron oxide nanoparticles have narrow size distribute within the range of about 10-15 nm. Which are well match with calculated value and was calculated it from Debye-Scherrer equation.

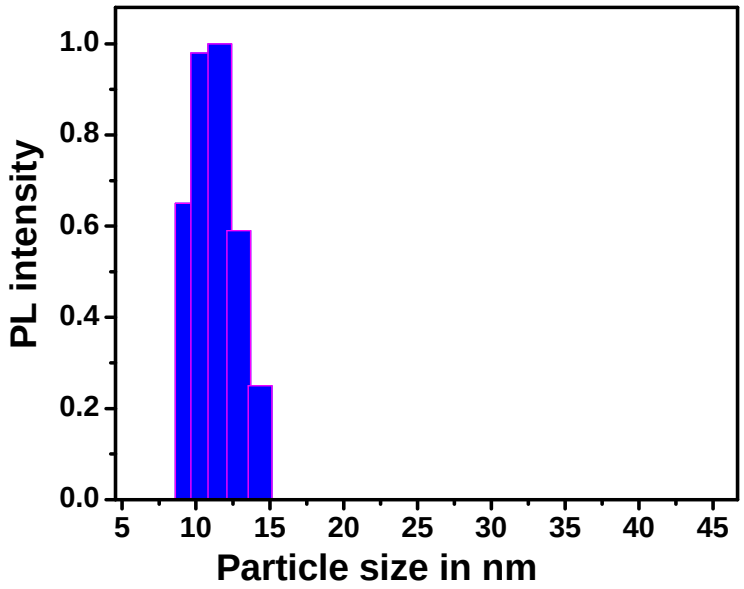

Fig. 4. Particle size distribution studies.

3.4. SEM Analysis

The microstructure of the sintered samples can be visualized from scanning electron microscope (SEM) tool. Fig. 5 Shown the particle morphology of high resolution, the particles are most irregular in shape with a Nanosize range. Some particles are found as agglomerations containing very fine particles the particles shapes are not defined porous nature and small and large core approximately (5 μm), spongy pores are seen in the micrograph. Porous material that is favorable to a gas sensing application.

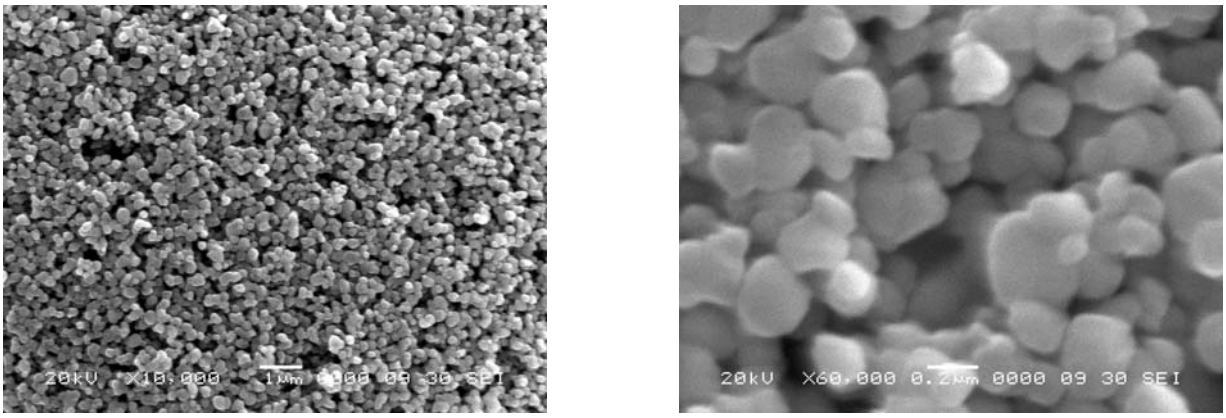

(a) (b)

Fig. 5. SEM images of mixed precursor at 800^{0}C in air for 4 h (a) low resolution and, (b) high resolution.

3.5. TEM Analysis

The detailed morphology and crystalline structure of the $MgFe_2O_4$ calcined at 700 and 800 ^{0}C for 4 h were further investigated by TEM, and the TEM bright-field images with corresponding selected-area electron diffraction (SAED) patterns of these two samples are shown in Fig. 6. It is clearly seen from the TEM bright field images that both samples consisted of packed $MgFe_2O_4$ particles or crystallites with particle sizes of ~10–20 and 25–80 nm in diameter for the samples of 700 ^{0}C-calcined and 800

^{0}C-calcined, respectively. It is seen that the particle sizes of$MgFe_2O_4$ contained in the calcined $MgFe_2O_4$ are quite uniform. Since the electro spun powder were very standard data (JCPDS: 88-1935). The diffraction rings are identified as the (111), (220), (311), (400), (422), (511), and (440) planes. This concurs with the results of XRD presented in Fig. 3.

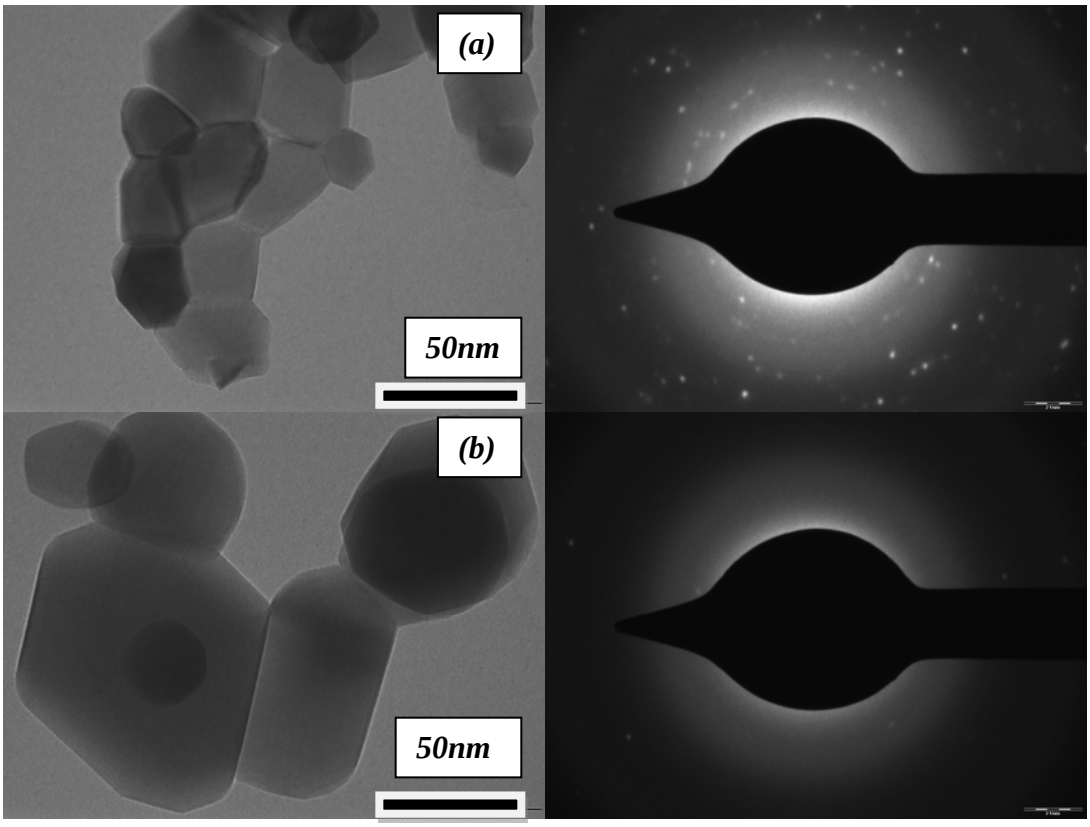

Fig. 6.TEM images with corresponding SAED patterns of the $MgFe_2O_4$samples calcined in air for 4h at (a)700 ^{0}C and (b) 800 ^{0}C.

3.6. FT-IR Analysis

The formation of spinel $MgFe_2O_4$ structure in the calcined$MgFe_2O_4$was further supported by FT-IR spectra (Fig. 7). Here, we consider two ranges of the absorption bands: 4000–1000 and 1000–400 cm^{-1} as suggested by previously published studies [41]. In the range of 4000–1000 cm^{-1}, vibrations ofCO_3^{2-} and moisture were observed. The intensive band at~~1627 cm^{-1} is due to O–H stretching vibration interacting through H bonds. The band at ~ 2920 cm^{-1} is C–Hasymmetric stretching vibration mode due to the $–CH_2–$groups of the long aliphatic alkyl groups. The υ(C=O)stretching vibration of the carboxylate group ($CO_2^{2-)}$ was observed around 1380 cm^{-1} and the band at ~1016 $cm^{-1}$was corresponded to nitrate ion traces. Therefore theCO_3^{2-} and CO_3^{-}vibrations disappeared when calcinations temperature was increased. In the range of 1000–400cm^{-1}, a typical metal–oxygen absorption band for the spinel structure of the ferrite at ~560 cm^{-1} was observed in the FT-IR spectra of all of the calcined $MgFe_2O_4$ samples. This band strongly suggests the intrinsic stretching vibrations of the metal (Fe ↔ O) at the tetrahedral site.

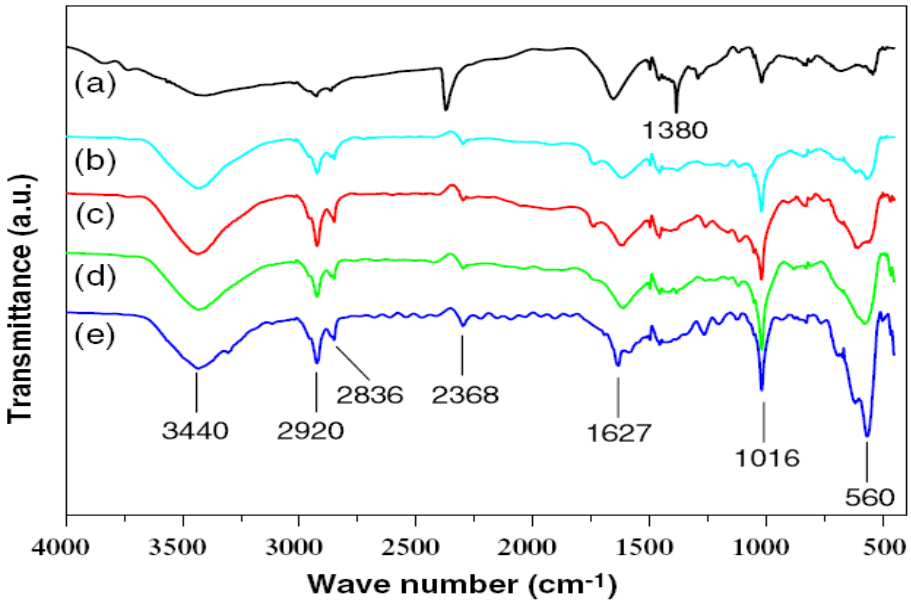

Fig. 7. FT-IR spectra of the $MgFe_2O_4$ composite samples calcined in air for 4 h at different temperatures (a) 180, (b) 500 ^{0}C, (c) 600 ^{0}C, (d) 700 ^{0}C, and (e) 800 ^{0}C.

4. Electrical Properties

4.1. I-V Characteristics

Fig. 8 depicts I-V characteristics of $MgFe_2O_4$films. It is clear from the symmetrical I-V characteristics that the silver contacts on the films were ohmic in nature.

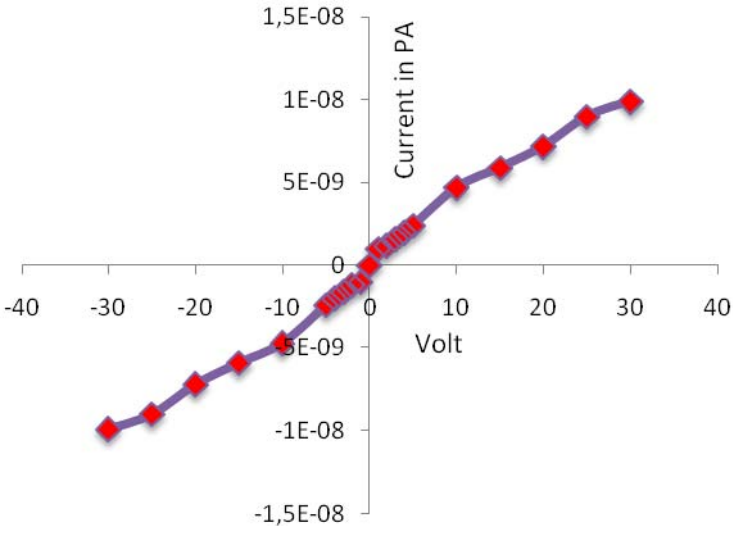

Fig. 8. *I-V* characteristics of the sensor.

4.2. Electrical Conductivity

Fig. 9 shows the variation of log (conductivity) with temperature. The conductivity values of sample increase with operating temperature. The increase in conductivity with increasing temperature could be

attributed to negative temperature coefficient of resistance and semiconducting nature of $MgFe_2O_4$. It is observed that the electrical conductivities of the $MgFe_2O_4$ films are nearly linear in the temperature range from 50-400 ^{0}C in air ambient. The room temperature conductivity of $MgFe_2O_4$ is 2.45×10^{-2} mho/m.

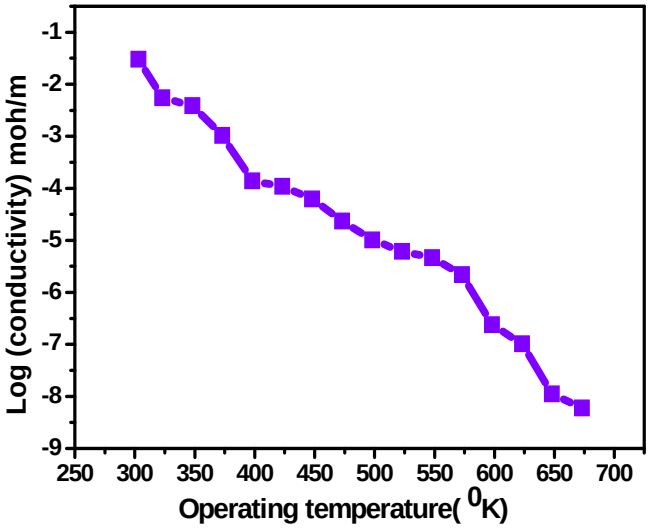

Fig. 9. Variation of Resistivity with reciprocal operating temperature.

5. Sensing Performance of the Sensor

5.1. Measurement of Gas Response, Selectivity, Response and Recovery Time

Gas response (S) is defined as the ratio of the change in conductance of the sensor on exposure to the target gas to the original conductance in air. The relation for S is as:

$$S = \frac{G_g - G_a}{G_a} \tag{3}$$

where G_a and G_g are the conductance of sensor in air and in a target gas medium, respectively.

Selectivity or specificity is defined as the ability of a sensor to respond to a certain gas in the presence of other gases. The time taken for the sensors to attain 90 % of the original conductance is the recovery time.

5.2. Sensing Performance of Pure $MgFe_2O_4$ Thick Film

5.2.1. Effect of Operating Temperature

Fig. 10 depicts the variation of response to ethanol (30 ppm) with operating temperature of $Mg_2Fe_2O_4$ thick films. The largest response of $MgFe_2O_4$ was observed to be 1.96 % at room temperature. The ethanol response at room temperature is expected to be monitored by adsorption of moisture on the $MgFe_2O_4$ film. The cumulative effect would decrease the film resistance, giving a response to ethanol gas at room temperature. At room temperature, there would be no oxygen adsorption. Therefore, the oxygen adsorption-desorption mechanism is not employed to sense the ethanol gas.

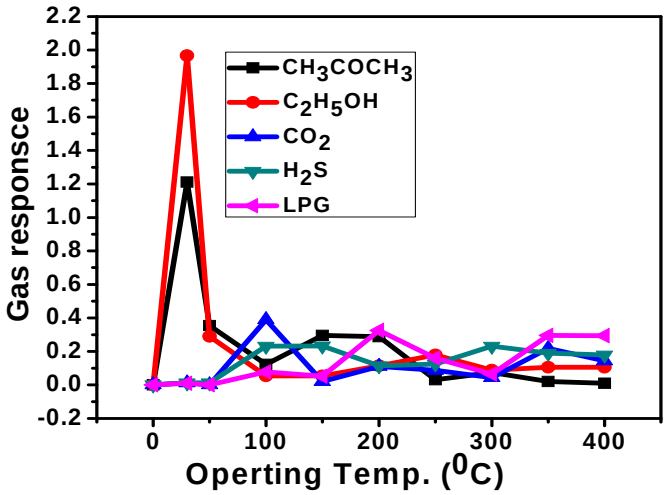

Fig. 10. Variation of gas response of $MgFe_2O_4$with operating temperature.

5.3.2. Effect of Ethanol Gas Concentration at Room Temperature (Active Region)

The variation of gas response of the $MgFe_2O_4$ sample with ethanol gas concentration at room temperature is represented in Fig. 11 this film was exposed to varying concentrations of ethanol gas for $MgFe_2O_4$ samples, the response values were observed to increase continuously with increasing the gas concentration up to 1000 ppm at room temperature. The rate of increase in response was relatively larger up to 30 ppm, but smaller during 30 and 1000 ppm. Thus, the active region of the sensors would be up to 30 ppm. At lower gas concentration, the unimolecular layer of gas molecules would be formed on the surface of the sensor which could interact more actively giving larger response. The multilayer of the gas molecules on the sensor surface, at the higher gas concentration, would result into saturation in response beyond 30 ppm gas.

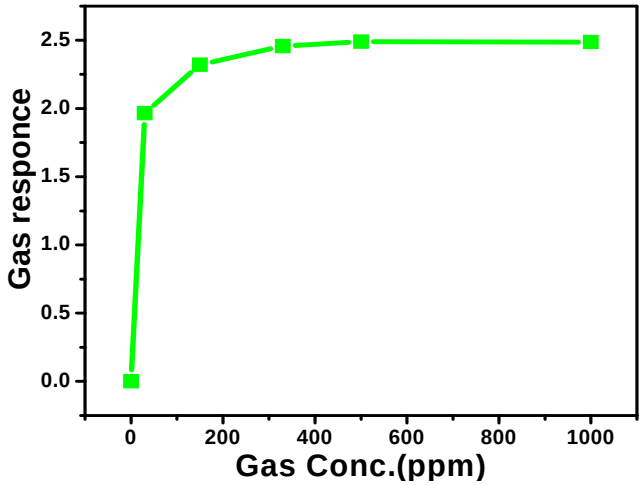

Fig. 11. Variation of gas response with gas concentration.

5.3.3. Selectivity for Ethanol Against Various Gases

Fig. 12 depicts the selectivity of the MgF_2O_4 sensor for ethanol (30 ppm) gas at room temperature. The sensor showed high selectivity to ethanol against other gases (1000 ppm) acetone, CO_2, H_2S, LPG gases.

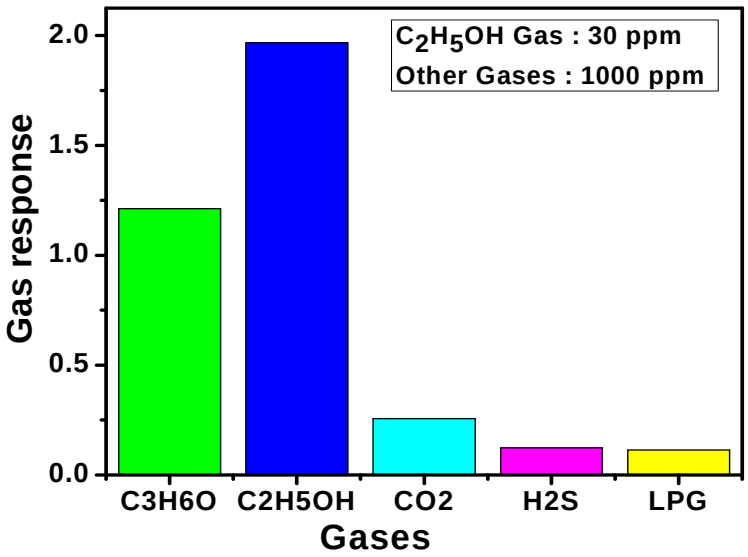

Fig. 12. Selectivity of $MgFe_2O_4$ thick film among various gases.

5.3.4. Response and Recovery of the Sensor

Fig. 13 depicts the response and recovery of the $MgFe_2O_4$ sensor. The response was quick (~ 20 s) to 30 ppm of ethanol, while the recovery was considerably fast (~ 60 s). A negligible quantity of the surface reaction product and its volatility explain its quick response to ethanol and fast recovery to its initial chemical status.

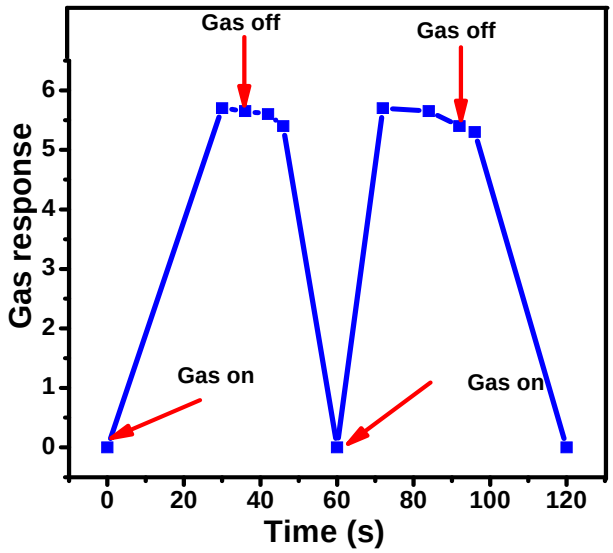

Fig. 13. Response and recovery of the sensors.

5.3.5. Response at Room Temperature

Gas sensing mechanism is generally explained in terms of conductance change either by adsorption of atmospheric oxygen on the surface and/or by direct reaction of lattice oxygen or interstitial oxygen with test gases. In the former case, the atmospheric oxygen adsorbs on the surface by extracting electrons from the conduction band to form superoxides or peroxides, which are mainly responsible for

the detection of the test gases. The $MgFe_2O_4$ thick films cause the formation of inter grain boundaries of $MgFe_2O_4$-$MgFe_2O_4$ grains. The exposed ethanol gas molecule captures the lattice oxygen from the surface of the film at room temperature. This would result the oxygen deficiency in the bulk of the material preferably at the surface. The semiconductivity in $MgFe_2O_4$ may be due to large oxygen deficiency. The increase in the conductivity of $MgFe_2O_4$ thick film could be attributed to the charge-carrier generation mechanism resulted from the electronic defects due to nanostructured size of the grains. These generated electrons and the donor level in the energy band gap of $MgFe_2O_4$ will contribute to increase in conductivity. This results in increasing the conductance of the film at room temperature.

6. Conclusion

1. A nitrate gel synthesized from metal nitrate and glycine by sol-gel process with molar ratio of 1:1 exhibits auto combustion behavior. The auto combustion method proves good for the synthesis of nano-sized magnesium ferrites.
2. The phage formation of the MgFe2O4 is investigated by TG-DTA, XRD, FT-IR techniques. The synthesized product shows single phage of inverse spinel structure with an average diameter 10-15 nm.
3. The sensor was highly selective to ethanol gas (30 ppm) against other toxic gases of higher concentrations.
4. The sensor showed very rapid response (~ 20 s) and recovery (~60 s) to ethanol gas.
5. The sensor has good selectivity to ethanol gas against acetone, CO2, H2S and LPG gases.

Acknowledgement

The author S. V. Bangale is thankful to IIT Bombay for providing the TEM facility during this research work.

References

[1]. M. Sugimoto, *J. Am. Ceram. Soc*., 82, 1999. pp. 269.
[2]. Y. Liu, Z. M. Liu, Y. Yang, H. F. Yang, G. L. Shen, R. Q. Yu, *Sensors and Actuators,* B, 107, 2005. pp. 600-604.
[3]. P. P. Hankare, S. D. Jadhav, U. B. Sankpal, R. P. Patil, R. Sasikala, I. S. Mulla, Electromagnetic Studies of Nickel Ferrite Synthesized by Microwave, *Journal of Alloys and Compounds,* 488, 2009, pp. 270-272.
[4]. R. J. Willey, P. Noirclerc, G. Busca, *Chem. Eng. Commun.*, 123, 1993.
[5]. S. A. Oliver, R. J. Willey, H. H. Hamdeh, G. Oliveri, G. Busca, *Scr. Mater*., 33, 1995. pp. 1695.
[6]. W. Wu, Q. He, C. Jiang, Synthesis of magnetic and fluorescent multifunctional hollow Nanoscale, *Nanoscale Res. Lett.,* 3, 2008, pp. 397.
[7]. Z. H. Hua, R. S. Chen, C. L. Li, S. G. Yang, M. Lu, X. B. Gu, Y. W. Du, CoFe2O4 nanowire arroys prepared by template electrodepositio method and further oxidation, *J. Alloys Compd*., 427, 2007, pp. 199.
[8]. S. A. Corr, Y. P. Rakovich, Y. K. Gun'ko, Multifunctional Magnetic-fluorescent Nanocomposites for Biomedical Applications, *Nanoscale Res. Lett.,* 3, 2008, pp. 87.
[9]. Z. Lai, G. Xu, Y. Zheng, *Nanoscale Res. Lett.,* 2, 2007, pp. 40.
[10]. C. V. Gopal Reddy, S. V. Manorama, V. J. Rao, Preparation and characterization of ferrites as gas sensor materials*, J. Mater. Sci. Lett*., 19, 2000. pp. 775.
[11]. N. Xinshu, L. Yanli, X. Jiaqiang, Simple synthesis of $MgFe_2O_4$ nanoparticles as gas sensing materials, *Chin. Funct. Mater*., 33, 2002. pp. 413.
[12]. L. Satyanarayana, K. Madhusudan, Reddy, V. M. Sunkara, Nanocrystallinespinel $Ni_{0.6}Zn_{0.4}Fe_2O_4$: A novel material for H_2S, *Chem. Phys*., 82, 2003. pp. 21.

[13].C. Liu, B. Zou, A. J. Rondinone, Z. J. Zhang, Characterization of nanosized NiZn ferrite powders synthesized, *J. Am. Chem. Soc.,* 122, 2000, pp. 6263.
[14].G. Busca, E. Finocchio, V. Lorenzelli, M. Trombetta, S. A. Rossini, *J. Chem. Soc. Faraday Trans*., 92, 1996. pp. 4687.
[15].Y. Shimizu, H. Arai, T. Seiyama, *Sens. Actuators,* 7, 1985, pp. 11.
[16].F. A. Benko, F. P. Koffyberg, *Mater. Res. Bull.,* 21, 1986, pp. 1183.
[17].M. Sugimoto, The past, present, and future of ferritess, Dependence of magnetic and structural properties of $Ni_{0.5}$ $M_{0.5}$, *J. Am. Ceram. Soc.,* 82, 1999. pp. 269-280.
[18].R. B. Kamble, V. L. Mathe, Nanocrystalline nickel ferrite thick film as an efficient gas**,** *Sens. Actuators,* 131, 2008, pp. 205-209.
[19].R. D. McMichael, R. D. Shull, L. H. Bennett, R. E. Watson, Magnetocaloric effect in superparamagnets, *J. Mang. Mater,* 11, 1992, pp. 29-30.
[20].C. V. Gopal Reddy, S. V. Manorama, V. J. Rao, Preparation and characterization of ferrites as gas sensors materials, *J. Mater. Sci. Lett.,* 9, 2000, pp. 775-778.
[21].N. S. Chen, X. J. Yang, E. S. Liu, J. L. Huang, Reducing gas-sensing properties of ferrite compounds MFe_2O_4 (M= Cu, Zn, Cd, and Mg), *Sens. Actuators B,* 66, 2000, pp. 178180.
[22].E. Rezlescu, P. D. Popa, N. Rezlescu, gas sensitivity of nanocrystalline nickel ferrite, thermal of optoelectronic and advanced materials, *Sens. Actuators B,* 8, 3, 2006, pp. 1016.
[23].T. W. Solomans, C. B. Fryhale, Organic Chemistry, 8th ed., 2004, pp. 497.
[24].G. S. Sodi, Fundamental concepts of enveriomental chemistry, *Narosa Publishing House*, New Delhi, 2002, pp. 135.
[25].S. M. Khetre, H. V. Jadhav, P. N. Jagdale, S. V. Bangale, S. R. Bamane, Use of mixed metal oxideas a catalyst in the decomposition of H_2O_2, *Advances in Applied Science Research*, 2, 2011, pp. 252-259.
[26].T. Kodama, Y. Wada, T. Yamamoto, M. Tsuji, Y. Tamaura, *J. Mater. Chem*., 5, 1995. pp. 1413.
[27].S. Hirano, T. Yogo, K. Kikuta, E. Asai, K. Sugiyama, H. Yamamoto, Simple synthesis of $MgFe_2O_4$ nanoparticles as gas sensing materials, *J. Am. Ceram. Soc*., 76, 1993, pp. 1788.
[28].J. F. Hochepied, P. Bonville, M. P. Pileni, Nonstoichiometric Zinc Ferrite Nanocrystals: Syntheses and Unusual, *J. Phys. Chem. B,* 104, 2000, pp. 905.
[29].M. Kiyama, Synthesis and characterization of ultrafine Mn (II)-bearing, *Bull. Chem*., 51, 1978, pp. 134.
[30].S. Verma, P. A. Joy, Y. B. Khollam, H. S. Potdar, S. B. Deshpande, Microwave hydrothermal synthesis and visible-light photocatalytic activity of Bi_2WO_6 nanoplates, *Mater. Lett*., 58, 2004, pp. 1092.
[31].M. J. Madon, S. R. Morrison, Chemical Sensing in Solide State Devices, *Academic Press,* San Diago, 1989.
[32].K. N. P. Kumar, A. Keizer, A. J. Burggraaf, T. Okubo, H. Nagamoto, S. Morooka, *Nature,* 48, 1992, pp. 358.
[33].G. Sberveglirri, L. E. Depero, M. Ferroni, V. Guidi, G. Martinelli, P. Nelli, C. Perego, L. Sangletti, *Adv. Mater*., 8, 1996, pp. 334.
[34].S. V. Bangale, D. R. Patil, S. R. Bamane, Preparation and electrical properties of nanocrystalline $MgFe_2O_4$ oxide by combustion route, *Archives of Applied Science Research*, 3, 2011, pp. 506-513.
[35].S. V. Bangale, S. M. Khetre, S. R. Bamane, Preparation and electrical properties of nanocrystalline $ZnFe_2O_4$ oxide by combustion route, *Der Chemica Sinica*, 2, 2011, pp. 303.
[36].D. R. Patil, L. A. Patil, P. P. Patil, Cr_2O_3-activated ZnO thick film resistors for ammonia gas sensing operable at room temperature *Sensors and Actuators,* B, 126, 2007, pp. 368–374.
[37].B. D. Cullity, S. R. Stock, Elements of X-ray Diffraction, *Prentice Hall,* NJ, 2001.
[38].C. Hammond, The Basis of Crystallography and Diffraction, *Oxford University Press,* Oxford, 1997.
[39].Y. Huang, Y. Tang, J. Wang, Q. Chen, *Mater. Chem. Phys*., 97, 2006, pp. 394.
[40].S. Maensiri, M.Sangmanee, A.Wengmoon, Magnesium Ferrite ($MgFe_2O_4$) Nanostructures Fabricated by Electrospinning, *Nanoscale Res Lett*. 2009, 4(3), pp 221–228.
[41].G. V. S. Rao, C. N. R. Rao, J. R. Ferraro, Studies on the catalytic decomposition of N_2O on $LnSrFeO_4$ (Ln=La, Pr, Nd, Sm and Gd), *Appl. Spectrosc*., 24, 1970, pp. 436.
